High throughput screening of monoamine oxidase (MAO-N-D5) substrate selectivity and rapid kinetic model generation

L. Rios-Solis [a,b], B. Mothia [a], S. Yi [a], Y. Zhou [a], M. Micheletti [a], G.J. Lye [a,*]

[a] The Advanced Centre for Biochemical Engineering, Department of Biochemical Engineering, University College London, Gordon Street, London WC1H 0AH, UK
[b] Faculty of Pharmacy, Autonomous University of the State of Morelos, Av. Universidad 1001, Col. Chamilpa, Cuernavaca, Morelos 62209, Mexico

ABSTRACT

Full kinetic models provide insight into enzyme mechanism and kinetics and also support bioconversion process design and feasibility assessment. Previously we have established automated microwell methods for rapid data collection and hybrid kinetic modelling techniques for quantification of kinetic constants. In this work these methods are applied to explore the substrate selectivity and kinetics of monoamine oxidase, MAO-N-D5, from *Aspergillus niger*. In particular we examine the MAO-N-D5 variant Ile246Met/Asn336Ser/Met348Lys/Thr384Asn to allow the oxidation of secondary amines Initial screening showed that MAO-N-D5 enabled the selective oxidation of secondary amines in 8 and 9 carbon rings, as well as primary ethyl and propyl amines attached to secondary amines of indolines and pyrrolidines. Subsequently we developed a first kinetic model for the MAO-N-D5 enzyme based on the ping-pong bi-bi mechanism (similar to that for the human MAO-A enzyme). The full set of kinetic parameters were then established for three MAO-N-D5 substrates namely; 3-azabicyclo[3,3,0]octane, 1-(2 amino ethyl) pyrrolidine and 3-(2,3-dihydro-1H-indole-1-yl)propan-1-amine. The models for each amine substrate showed excellent agreement with experimentally determined progress curves over a range of operating conditions. They indicated that in each case amine inhibition was the main determinant of overall reaction rate rather than oxygen or imine (product) inhibition. From the perspective of larger scale bioconversion process design, the models indicated the need for fed-batch addition of the amine substrate and to increase the dissolved oxygen levels in order to maximize bioconversion process productivity.

© 2015 The Authors. Published by Elsevier B.V. This is an open access article under the CC BY license (http://creativecommons.org/licenses/by/4.0/).

1. Introduction

Biocatalytic processes are increasingly being considered in industrial organic syntheses since in certain situations they are considered 'greener' and can bring considerable reductions to overall process costs [1,2]. This is a consequence of the mild temperature, pressure and pH conditions under which enzymes function. Their high regio- and stereo selectivity facilitates conversions with high atom efficiency and reduced environmental impact [3].

To develop a biocatalyst for commercial application, even after several rounds of successful protein engineering or evolution, it is still necessary to screen several enzyme variants with a variety of substrates over a range of concentrations [4,5]. In addition, it is useful to establish enzyme kinetic mechanisms and full kinetic models. These give fundamental insights into bioconversion operation and enable different reactor operating strategies to be simulated in order to determine process feasibility and cost effectiveness [6,7]. Nevertheless, most reported bioconversion kinetic studies only report the maximum reaction rate, V_{max}, and the Michaelis constant, K_m, along with qualitative comments on the level of substrate and/or product inhibition. This is because obtaining a full kinetic model along with values of all the inhibition constants involves multiple experiments and complex data processing, consuming valuable time and resources [8].

Recently, we have developed more rapid numerical techniques for enzyme kinetics determination that combine traditional initial rate experiments, to identify a solution in the vicinity of the global minimum, with non-linear regression methods to determine the exact location of the solution. These greatly reduce the number of experiments required to obtain the full set of kinetic parameters [9,10]. These numerical techniques have been combined with the creation of automated, microwell scale methods that increase the throughput and reduce the costs and timescales associated with experimental studies [11,12]. In the biocatalysis field, these microscale tools have been successfully applied to evolve, screen and characterize a broad range of enzymes [13,14]. We have also

shown how the results obtained at microwell scale can be used to predict fermentation and bioconversion kinetics at laboratory and pilot scale [15,16].

In this work we applied these methods to study the kinetics of the monoamine oxidase, MAO-N-D5, which is a homo dimer flavin dependant enzyme that catalyses the oxidation of amines [17]. Interest has arisen in the MAO-N-D5 enzyme due to its 49.1 and 48.7% sequence homology to the human monoamine oxidases MAO-A and MAO-B, which are responsible for oxidizing important neurotransmitters such as serotonin and dopamine [18]. MAO-N-D5 has previously been found to possess a high catalytic rate and selectivity with many aliphatic and aromatic amines [19,20]. The particular enzyme variant studied here has been subject to in vitro evolution, and the mutant Ile246Met/Asn336Ser/Met348Lys/Thr384Asn has been shown to facilitate the selective oxidation of secondary and tertiary amines [21–23]. The aim of this work is to further examine the substrate selectivity of the MAO-N-D5 mutant and to establish the first full kinetic models of the enzyme for conversion of a range of substrates. These will provide important insights into bioconversion process design and scale-up.

2. Materials and methods

2.1. Materials and plasmid

Molecular biology enzymes were obtained from New England Bio-laboratories (NEB, Hitchin, UK). Competent *Escherichia coli* BL21-Gold (DE3) cells were obtained from Stratagene (Amsterdam, Netherlands), while One Shot® *E. coli* BL21 Plyss and One Shot® *E. coli* BL21 Plyse cells were obtained from Invitrogen (Paisly, UK). Primers and oligonucleotides were purchased from Operon (Cologne, DE). All other reagents were obtained from Sigma–Aldrich (Gillingham, UK) unless noted otherwise, and were of the highest purity available.

Plasmid pET16b MAO-N-D5 contained the *Aspergillus niger* MAO-N-D5 gene with the following mutations: Ile246Met/Asn336Ser/Met348Lys/Thr384Asn [24], and was kindly provided by Professor Nick Turner (University of Manchester, UK). DNA sequencing was performed by the UCL Wolfson Institute for Biomedical Research. 12 µl of DNA sample were provided at a concentration of 100 ng µl^{-1} in 1.5 ml Eppendorf tubes. The primers used are shown in Table 1. Primers were commercially synthetized (Eurofins MWG Operon, London, UK) and prepared at a concentration of 5 pmoles l^{-1}. Sequencing results were routinely analyzed using Bioedit software (www.mbio.ncsu.edu/BioEdit/bioedit.html).

2.2. Synthesis of product imine 3-azabicyclo-[3,3,0]oct-2-ene

3-Azabicyclo[3,3,0]octane hydrochloride (**7**) (Table 2) (3.07 g, 21.0 mmol) was dissolved in 100 ml dichloromethane (DCM) and *N*-chlorosuccinimide (6.45 g, 48.3 mmol, 2.3 equiv) was added in one portion. The mixture was stirred for 1.5 h at room temperature and subsequently filtered. The filtrate was reduced to a volume of 20 ml, where precipitation occurred. The filtration was repeated, the precipitate was extracted with a small amount of DCM (5–7 ml) and the combined filtrates were added to a solution of KOH (2.41 g, 43.0 mmol, 2.04 mmol) in 50 ml methanol (MeOH). The turbid mixture was stirred overnight and filtered. The crude product was purified by flash column chromatography (hexane: EtOAc 9:1 followed by CH$_2$Cl$_2$: MeOH 99:1) to give the product 3-azabicyclo-[3,3,0]oct-2-ene (**17**) as yellow crystals (0.25 g, 2.29 mmol, 10%), identical by NMR with the literature [25].

2.3. Shake flask MAO-N-D5 fermentations and lysate preparation

Competent *E. coli* BL21-Gold (DE3), *E. coli* BL21 Plyse and *E. coli* BL21 *Plysee* cells were transformed with the plasmid pET16b MAO-N-D5 using the heat shock technique described by the supplier (Stratagene, Amsterdam, NL). An overnight culture of the transformed cells was produced in a 100 ml shake flask (10 ml working volume) of LB broth (10 g l^{-1} tryptone, 5 g l^{-1} yeast extract, 10 g l^{-1} NaCl) containing 150 mg ml^{-1} ampicillin. Growth was performed at 30 °C with orbital shaking at 250 rpm using an SI 50 orbital shaker (Stuart Scientific, Redhill, UK). The total volume of this culture was used to inoculate a 1 l shake flask (100 ml working volume) which was left to grow for 8 h. After 4 h, IPTG was added to a concentration of 0.5 mM for enzyme induction. Following the removal of broth by centrifugation, the cells were resuspended in 1 M phosphate buffer, pH 7.8 and used for whole cell bioconversions. When MAO-N-D5 lysate was needed, the cells were sonicated with a Soniprep 150 sonicator (MSE, Sanyo, Japan). The lysate suspension was centrifuged at 5000 rpm in Falcon tubes for 5 min. The clarified lysate was either used immediately or stored at −20 °C.

2.4. High throughput platform and microscale bioconversions

A Tecan Genesis platform (Tecan, Reading, UK) was used to perform the bioconversions in polypropylene 96-deep square well plates (DSW) (Becton Dickenson, NJ, USA) covered with a thermo plastic elastomer cap designed to work with automated equipment (Micronic, Lelystad, Netherlands). The automated platform included an integrated Thermomixer Comfort Shaker (Eppendorf, Cambridge, UK), with a shaking frequency and diameter of 400 rpm and 6 mm respectively, which was used to ensure homogeneous enzyme and temperature distribution. It also included a microplate centrifuge (Hettitch Rotanta 46 RSC, Tuttlingen, Germany) and an Ultraspec 1100 Pro UV/Visible microplate spectrophotometer (Amersham Biosciences, Buckinghamshire, UK) for absorbance measurements [26].

In a standard microscale bioconversion the total volume was 600 µl which comprised 300 µl of the MAO-N-D5 resuspended cell solution and 300 µl of a 40 mM solution of the selected substrate in 1 M phosphate buffer at pH 7.8. The plates were incubated at 37 °C with all experiments performed in triplicate. In individual experiments the biocatalysts form (whole cell or lysate), substrate type and concentration and buffer concentration were varied as indicated in the text. Samples (100 µl) were either withdrawn or whole wells were sacrificed for analysis as required.

In order to investigate oxygen availably during bioconversions, the dissolved oxygen tension (DOT) was measured in a specially adapted 96-DSW plate. A fluorescent oxygen sensor spot (Pst3, Pre-Sens – Precision Sensing GmbH, Germany) was mounted flush with the inside wall of a single well. The sensor spot was connected to a light emitting diode and photodetector (OXY-4, PreSens) via an optical fibre (PreSens) attached through the outside wall inline with the sensor spot. DOT measurements were taken every 15 s. Before each run, the sensor was calibrated at 0% air saturation at 30 °C after blanketing the plate with nitrogen for a period of 10 min. The calibration at 100% air saturation was similarly performed at 30 °C after pumping air over the well.

2.5. Analytical methods

Gas chromatography (GC) analysis was performed on a Trace 130 Gas Chromatograph (Thermo Scientific, UK) with a Thermo Scientific AS 1310 Autosampler, an instant Connect-FID flame ionization detector on a CAM column (30 m × 0.32 mm × 0.25 µm, J&W Scientific, Agilent Technologies). In order to carry out GC analysis, aliquots of 100 µl were withdrawn at various time intervals from

Table 1
Primer sequences used for sequencing the MAO-N-D5 gene.

Primer	Sequence
MAO forward:	5′-*CCAGGGACCAGCAATGACCTCCCGAGACGGATACCAG*-3′
MAO reverse:	5′-*GAGGAGAAGGCGCGTTATCACAAACGAGCCTTCACCTCC*-3′

the bioconversion solution and quenched with 10 μl of a 1 M NaOH solution. 200 μl *tert*-butyl methyl ether was added to the samples which were incubated at 37 °C and 900 rpm for 30 min in a Thermomixer Comfort shaker. The samples were then centrifuged for 5 min at 5000 rpm and the organic phase was collected for analysis. The injector temperature was set at 250 °C with triple times of pre-wash and post-wash setting. The split injection was set as 50:1. Measurements were carried out using the FID detector at constant flows 1.6 ml min^{-1} of He, 45 ml min^{-1} of H$_2$ and 350 ml min^{-1} of air at 250 °C. Measurements were controlled and recorded by Chromeleon® software (version: 7.1.2.1478, Dionex Cor., Sunnyvale, CA, 2013).

Substrate and product concentrations were quantified by GC based on their peak areas and calibration curves prepared for the individual compounds. For the standard bioconversion the retention times for substrate **7** and its corresponding imine 3-azabicyclo-[3,3,0]oct-2-ene (**17**) were 5.85 min and 6.87 min respectively. Protein and enzyme concentrations were determined using the Bradford assay and SDS-PAGE as described previously [27]. Enzyme specific activities were determined from the GC samples as the amount of imine product formed per unit of time normalized by the dry cell weight of *E. coli* biomass (or enzyme units) used in the reaction. One unit of enzyme activity was defined as the amount of enzyme which catalyzed the formation of 1 μmol of 3-azabicyclo-[3,3,0]oct-2-ene (**17**) for 1 min in a forward reaction at a 20 mM concentration at 37 °C, 400 rpm and a pH of 7.8, using a 1 M phosphate buffer.

^{1}H NMR spectra for the imine product 3-azabicyclo-[3,3,0]oct-2-ene (**17**) was recorded on a Bruker AVANCE III 600 (600 MHz) using CDCl$_3$ solvent. The chemical shifts (δ) were given in ppm units relative to tetramethylsilane, and coupling constants (J) are measured in Hertz. NMR: $_{\delta H}$(600 MHz, CDCl$_3$), 7.30 (1 H, m), 4.05 (1 H, dddd, J = 7.8, 4.2, 3.0, 1.8 Hz), 3.52 (1 H, dq, not fully resolved, J = 10.8, 2.4 Hz), 3.29 (1 H, m), 2.66 (1 H, m), 1.70–1.20 (7 H, 4 m). Chemical ionization (CI) mass spectra were recorded on a Thermo Finnegan MAT 900XP spectrometer. MS: (CI$^+$), C$_7$H$_{11}$N, *m/z:* 110.1 [M+H]$^+$.

2.6. Kinetic parameter determination

We have previously described a series of methodologies and numerical techniques for rapid kinetic parameter estimation [10,28]. These were implemented here using a programme developed in Matlab® software (MathWorks, Natick, MA, USA) in order to automatically perform all the non-linear regressions and statistical analyses. Non-linear regressions were performed using the mesh adaptive pattern search algorithm in Matlab® known as: "The Genetic Algorithm and Direct Search Toolbox". This method was previously shown to be more likely to achieve global optimization than gradient-based methods [28].

3. Results and discussion

3.1. Biocatalyst production and choice of host strain

Leaky expression of the selected MAO-N-D5 enzyme variant had the potential for intracellular toxicity effects due to production of H$_2$O$_2$ while reacting with cell metabolites [29]. To the best of our knowledge the choice of host to avoid leaky expression has
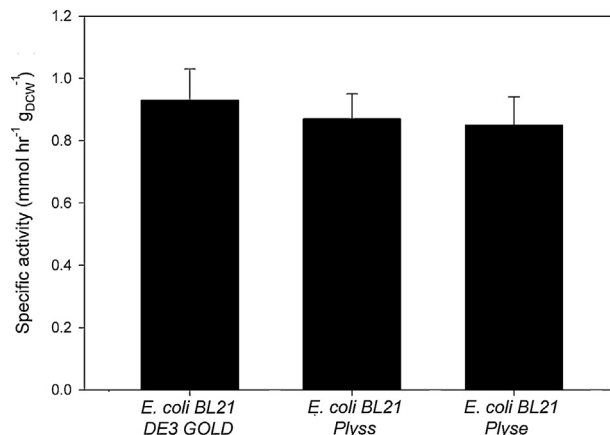

Fig. 1. Specific activity of MAO-N-D5 expressed in different *E. coli* strains. Growth of the various strains was performed in shake flasks as described in Materials and Methods section. Activities based on conversion of the substrate 3-azabicyclo [3.3.0] octane (**7**). Error bars represent one standard deviation about the mean (*n* = 3).

not been previously investigated, hence the enzyme was initially expressed in three different hosts: *E. coli* BL21 DE3 gold, *E. coli* BL21 DE3 *plyss* and *E. coli* BL21 DE3 *plyse*. These were selected due to their potentially different expression levels and degree of control of recombinant enzyme expression [30]. Enzyme activity was quantified using the standard substrate (**7**), previously shown to be successfully oxidized by the selected MAO-N-D5 variant to produce imine 3-azabicyclo-[3,3,0]oct-2-ene (**17**), which is an intermediate in the production of telaprevir drug for treatment of Hepatitis C [25].

Fig. 1 shows the specific MAO-N-D5 activity quantified using the different strains. No significant statistical difference was found between the different *E. coli* strains with all specific activities being in the range 1.05–1.2 mM min^{-1} g$_{DCW}$. Final biomass concentrations during the initial fermentations were also similar at 2.1, 1.8 and 1.7 g$_{DCW}$ l^{-1} for *E. coli* DE3 gold, *plyss* and *plyse* respectively. These levels of MAO-N-D5 specific activity are in agreement with literature results [22,25]. Therefore *E. coli* BL21 DE3 Gold was selected as the host strain for all further work due to the slightly higher cell concentrations produced during fermentation.

3.2. High throughput substrate and kinetics screening

Previous studies on the substrate selectivity of the MAO-N-D5 have reported that increasing the substrate bulk and lipophilicity led to higher rates of oxidation by the enzyme [25,29]. Consequently 16 different compounds were selected for activity screening based on structural variations of compound **7** used above. Modifications were considered that mainly related to the number and size of the carbon rings and various substitutions. Table 2 shows the structure of the selected amines and the measured activity levels. Compounds **5** and **11** were used as negative controls, as they were an amide and a fully oxidized heterocycle respectively, which theoretically could not be oxidized by MAO-N. Activity values are based on initial rates of product formation using a starting concentration of 20 mM of each substrate.

From the 16 compounds screened, compounds **3**, **4**, **7**, **8**, **13** and **14** resulted in a measurable rate of substrate conversion. The

Table 2
High throughput screening of the MAO-N-D5 mediated oxidation of various amines. All substrates screened at an initial concentration of 20 mM using 1.6 units of MAO-N-D5 in lysate form. Initial rates determined using the high throughput techniques described in the Materials and Methods Section. Dash indicates no measurable conversion after 40 h.
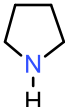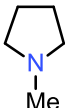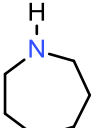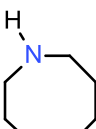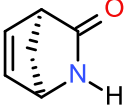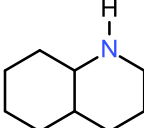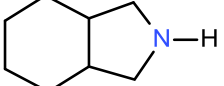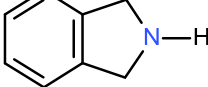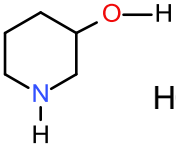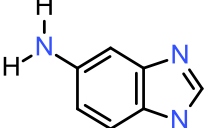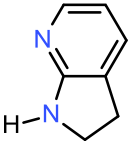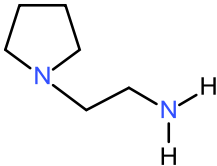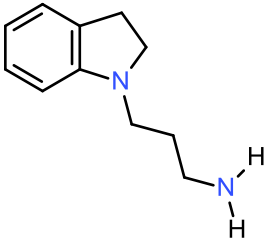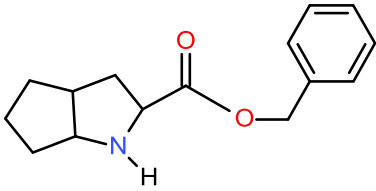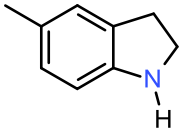
Substrate number	Name	Structure	Initial rate (mM h^{-1})
1	Pyrrolidine		–
2	1 Methyl pyrrolidine		–
3	Hexamethyleneimine		0.52
4	Heptamethyleneimine		0.15
5	2-Azabicyclo(2.2.1)hept-5-ene-3-one		–
6	Decahydroquinoline		–
7	3-Azabicyclo[3,3,0]octane		0.1
8	cis-8-azabicyclo[4.3.0] nonane		0.28
9	Indoline		–
10	3-hydroxy piperidine		–
11	5-Aminobenzimidazole		–

Table 2 (*Continued*)

Substrate number	Name	Structure	Initial rate (mM h^{-1})
12	2,3-Dihydro-7-azaindole		–
13	1-(2 amino ethyl) pyrrolidine		1.6
14	3-(2,3-dihydro-1H-indole-1-yl)propan-1-amine		0.2
15	Benzyl-2-azabicyclo[3.3.0]octane-3 carboxylate		–
16	5-Methylindoline		–

highest activity was found for compound **13** (1–2 amino ethyl pyrrolidine) while the lowest activity was for compound **7**. Compounds **1**, **2**, **7** and **8** have previously shown no activity with MAO-N-D5 in conventional labscale experiments and these results are confirmed here using the microwell platform [25].

As expected, negative control substrates 5 and 11 did not present any oxidation activity, and substrates **6**, **9**, **10**, **12**, **15** and **16** also showed that compounds containing a phenyl group gave no detectable activity. This could be due to phenyl groups being highly stable substituents, displaying steric hindrance and preventing any conversion taking place. The activity of MAO-N-D5 towards compounds **3**, **4**, **13** and **14** has not previously been reported in the literature. The results here demonstrate the capacity of the enzyme to oxidize secondary amines in rings with 8 and 9 carbons (compounds **3** and **4**), as well as primary ethyl and propyl amines attached to secondary amines of indolines and pyrrolidines (compounds **13** and **14**). These last two compounds are of particular interest since when the amine gets oxidized by MAO-N-D5, there is the potential to form new 5 and 6 membered heterocyclic compounds yielding the imines 3,5,6,7-tetrahydro-2H-pyrrolo[1,2-a]imidazole (**17**) and 2,3,4,10-tetrahydropyrimido-[1,2-a]indole (**18**) respectively as shown in Fig. 2. The identity of products **17** and **18** were confirmed by mass spectrometry and NMR.

Using the automated microwell platform further kinetic data was obtained in parallel on compounds **3**, **4**, **7**, **8**, **13** and **14** where initial rates of conversion were quantified as a function of initial substrate concentration. Michaelis–Menten profiles are shown in

Fig. 3 where, for ease of illustration, results are presented for the substrates demonstrating 'low' and 'high' activities respectively. Based on this data initial estimates of the maximum initial rate, V_{max}, and Michaelis constant, K_{amine}, were obtained for the six priority substrates as shown in Table 3. These results suggest that increasing the lipophilicity of the substrates results in higher MAO-N-D5 activity, which is in agreement with previous work [25].

The ability to collect this additional kinetic data on multiple substrates in parallel gives further insight to the screening results and also to issues of inhibition that will inform strategies for bioconversion process design [31]. The kinetic profiles in Fig. 3 indicate that the substrate concentration of 20 mM used in the initial screening experiments (Table 2) was already above inhibitory levels, e.g. for compounds **3** and **4** which was severely inhibited at 20 mM, or well below them e.g. for compound **14** where the activity at 100 mM was five times higher than in the screening experiments. These results reemphasise that quantification of enzyme activity at single substrate concentrations can often be misleading.

Structurally similar compounds **7** and **8** exhibited substrate inhibition above concentrations of 100 mM and while the V_{max} values were of the same order of magnitude, the K_m of compound **7** was five times smaller. Likewise, compounds **3** and **4** both showed significant substrate inhibition above concentrations of 10 mM. Both these substrates presented similar V_{max} values that were one order of magnitude higher than those of compounds **7** and **8**, while the K_m values were similar (with the exception of compound **8**). The V_{max} values of compounds **13** and **14** were 15 and 33 times higher than the reference substrate **7** although the K_m values were 2.5
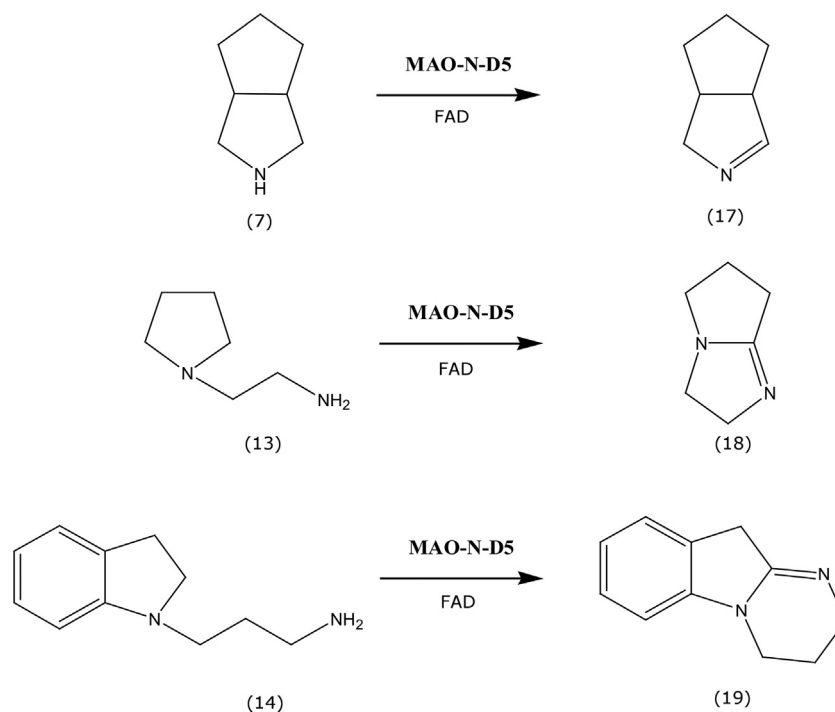
Fig. 2. Reaction scheme of the MAO-N-D5 mediated oxidation of compounds **7**, **13** and **14,** forming imine 3-azabicyclo-[3,3,0]oct-2-ene (**17**) and new imines with 5- and 6-membered heterocyclic rings: 3,5,6,7-tetrahydro-2H-pyrrolo[1,2-a]imidazole (**18**) and 2,3,4,10-tetrahydropyrimido-[1,2-a]indole respectively (**19**).

and 15 times higher respectively indicating lower binding affinity (Table 3).

In terms of progressing to a first full kinetic model for the MAO-N-D5 enzyme compound **7** was selected since this model substrate has been used in previous works where partial kinetic data has been gathered and is available for comparison [22,23]. Given the novelty of the products obtained from compounds **13** and **14,** kinetic models were also established for these two additional substrates. Derivates from compound **17** have been successfully used as catalysts for the synthesis of polyurethanes [32], while compound **18** is of special interest acting as a potential intermediate in the synthesis of heterocyclic amides used as anti-tumoral agents [33].

3.3. MAO-N-D5 mechanism and kinetic parameter determination

MAO-N-D5 belongs to a family of enzymes that catalyze the oxidation of monoamines using FAD as a cofactor [20]. Previous studies have shown that the MAO-N-D5 kinetic profile has more resemblance to the human MAO-A, which follows a ping–pong bi–bi mechanism, rather than to the human MAO-B which follows a bi–bi ordered reaction mechanism [17]. Based on this literature precedent a proposed King-Altman scheme for the MAO-N-D5 mediated oxidation of amines is shown in Fig. 4. The corresponding rate model is derived in Eq. (1).

$$v = \frac{V_{\max}([\text{Amine}][O_2])}{den} \tag{1}$$

Here $V_{\max}$ is the maximum reaction rate, K_{O_2} and K_{amine} are the corresponding Michaelis constants for O_2 and the amine substrate respectively, while $K_{i,\text{amine}}$, K_{i,O_2} and $K_{i,\text{imine}}$ are the corresponding inhibition constants for the amine substrate, O_2 and the resulting imine product. In the experiments required to determine those kinetic parameters, catalase (2.5 mg ml^{-1}) was added to the

bioconversions in order to avoid any build-up of H_2O_2 in the reaction mixture since it is known to be potentially damaging to the enzyme thus complicating kinetic measurements with issues of enzyme stability [23]. The in situ removal of H_2O_2 also has the benefit of removing the by-product making the reaction irreversible as shown in Fig. 4(A).

Because pH and dissolved oxygen fluctuations can affect the quality of the experimental data, and lead to determination of incorrect kinetic parameter values, these were first investigated in the microscale format used here for high throughput kinetic data collection. Fig. 5 shows the imine production curves for the MAO-N-D5 mediated oxidation of substrate **7** at an initial concentration of 20 mM. This figure also shows the pH and DOT measured in the microwell during the course of bioconversions at two different buffer concentrations.

Full conversion of substrate **7** is seen after 8 h in the bioconversion using 1 M phosphate buffer while the conversion using 100 mM buffer only reached 75% conversion in the same period. This difference is attributed to the significant decrease in reaction pH, from 7.8 to 6.0, observed when using the lower buffer concentration. Consequently all subsequent bioconversions were performed in 1 M phosphate buffer to ensure reaction kinetics were determined at a constant pH. Fig. 5 also shows that the measured DOT levels remained constant, at close to 100% saturation, for both bioconversions, demonstrating that the combination of liquid fill volume, well geometry and shaking diameter/frequency used

$$den = K_{O_2}[\text{Amine}]\left(1 + \frac{[\text{Amine}]}{K_{i,\text{amine}}}\right) + K_{\text{amine}}[O_2]\left(1 + \frac{[O_2]}{K_{i,O_2}}\right) + [\text{Amine}][O_2] + \frac{K_{\text{Amine}}}{K_{i,\text{imine}}}[O_2][\text{Imine}] + \frac{K_{\text{amine}}K_{iO_2}}{K_{i,\text{imine}}}[\text{Imine}]$$

[34] were sufficient to ensure that oxygen mass transfer into the microwell never became rate limiting.

Having verified the experimental system, the methodology established in our previous work was applied in order to rapidly
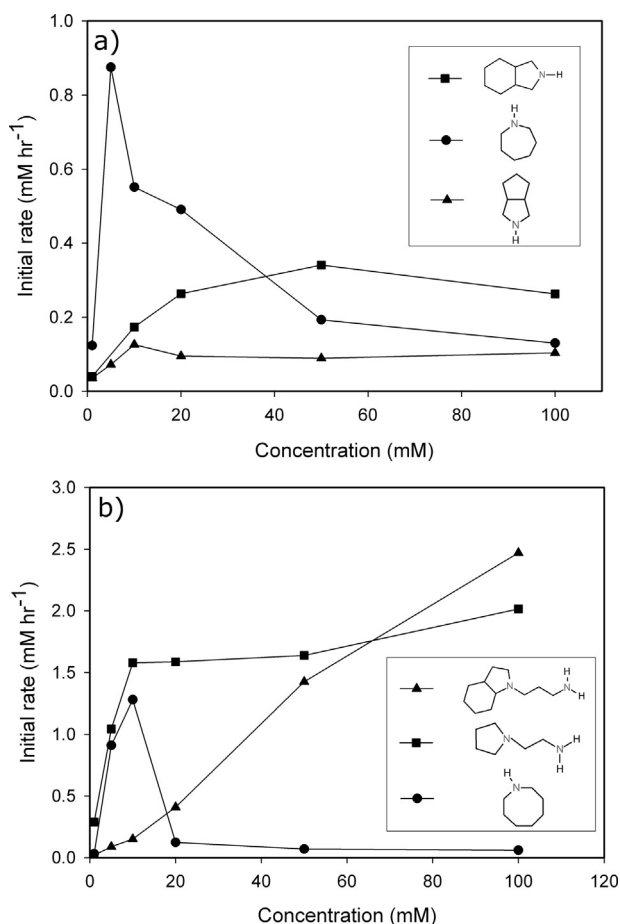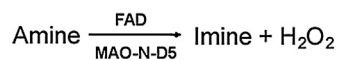
Fig. 3. Variation of MAO-N-D5 activity in lysate form with substrate concentration: (a) substrates with 'low' activity and (b) substrates with 'high' activity. Kinetics quantified using the high throughput techniques described in Section 2. Substrates in 1 M phosphate buffer pH 7.8, 37 °C and 400 rpm, 1.6 units of MAO-N-D5 were used in all reactions.

Fig. 5. Kinetics of whole cell MAO-N-D5 mediated oxidation of 3-azabicyclo[3,3,0]octane (7) in either 100 mM phosphate buffer (open symbols) or 1 M phosphate buffer (solid symbols): imine product concentration (△,▲), pH (○,●) and dissolved oxygen tension, DOT (□,■). Bioconversion conditions: 20 mM substrate, 15 g_{DCW} l^{-1} MAO-N-D5 whole cells, initial pH 7.8, 37 °C, 400 rpm, total volume of 0.6 ml in 96 well plates. Error bars represent one standard deviation about the mean ($n = 3$).

determine the kinetic constants for each of the three selected substrates [9,10]. Briefly this involves first performing traditional initial rate experiments at low concentrations to determine the Michaelis–Menten and rate constants, which represents values close to 'real solution'. This is combined with nonlinear regression methods applied to full progress curves at high substrate concentrations to determine the inhibition constants, as well as helping refine the exact location of the solution, improving the quality of the parameters while reducing the number of experiments required.

Here then, the appropriate experimental Michaelis–Menten parameters obtained in Table 3 were used as initial values to perform non-linear regression analysis with 15 progress curves for each substrate, at initial substrate concentrations between 50 and −300 mM, in order to determine the full set of kinetic parameters. At initial substrate concentrations higher than 100 mM, reactions with each of the 3 substrates did not reach full conversion, and no
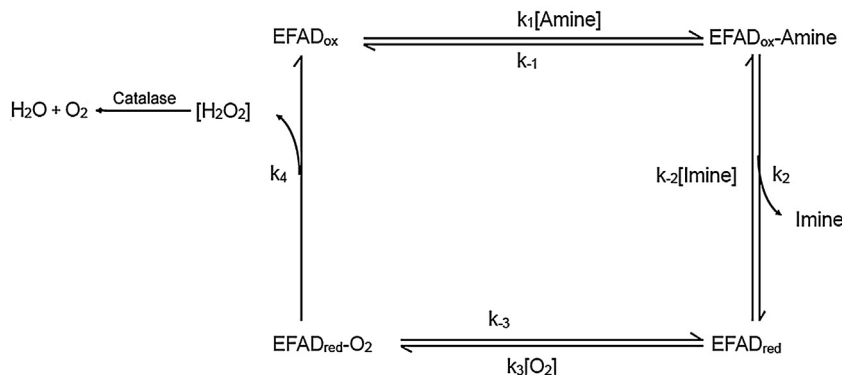

Fig. 4. Proposed King-Altman scheme of the MAO-N-D5 mediated oxidation of amines following a ping-pong bi-bi mechanism. EFAD$_{ox}$: enzyme bound to cofactor FAD in the oxidized form, EFAD$_{red}$: enzyme bound to cofactor FAD in the reduced form.
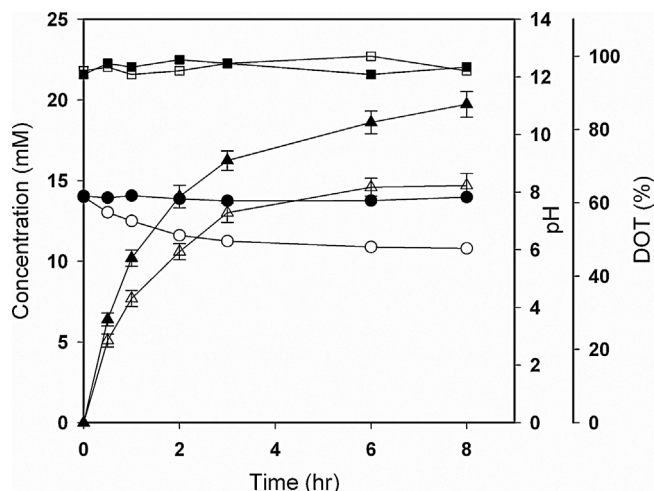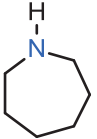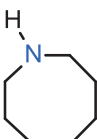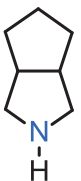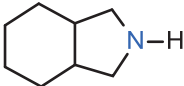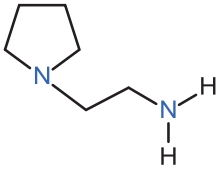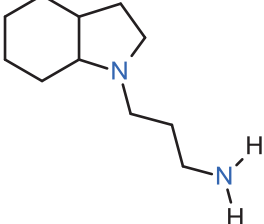
Table 3

Apparent V_{max} and K_m values determined for the MAO-N-D5 mediated oxidation of the selected amines shown in Fig. 3. Concentration of MAO-N-D5 was 1.6 units as defined in the Materials and Methods Section.

Substrate number	Structure	V_{max} (mM h^{-1})	K_m (mM)
3		1.2	3
4		1.4	4
7		0.16	4
8		0.42	18
13		2.5	10
14		5.3	60

increase in imine production was detected after 20 h bioconversion. Therefore the maximum duration of the progress curves used to determine the kinetic parameters was set to 20 h.

Because the dissolved O_2 concentration could only be monitored and not controlled in the standard microwells, Michaelis–Menten plots varying O_2 could not be experimentally obtained. The initial value for the Michaelis constant of O_2 (K_{O2}) was taken from previous studies of MAO-N-D5 that reported a value of 0.7 mM [17]. Using air as the O_2 source, the maximum concentration that could be reached in the microwell reactions at 37 °C was 0.21 mM [35], which is approximately four times lower than the literature K_{O2} value. The Michaelis–Menten profiles (Fig. 3) and kinetic parameters obtained from them (Table 3) will therefore be oxygen limited due to solubility limitations in the aqueous reaction media. In the current experimental set-up it was not possible to use pure oxygen instead of atmospheric air in the robotic containment cabinet, therefore the kinetic parameter values determined here will be apparent kinetic parameters suitable when using air as the oxygen source.

The final values determined for each of the apparent kinetic parameters in Fig. 4 are summarized in Table 4. Results are shown for each of the three selected substrates. For substrates 13 and 14, initial oxidation of the pyrrolidine ring by MAO-N leads to the

respective δ-1-pyrroline imine, which is followed by an attack of the primary amine side chain, resulting in the bicyclic derivative. Subsequently, another oxidation is required to obtain products 18 and 19. Further work needs to be performed in order to determine the exact reaction mechanism of this second oxidation. In this work, however, we have considered it to be oxygen mediated, and due to the slow rate of the first MAO-N oxidation and the excess of molecular oxygen, we have not included this step in the kinetic model.

Fig. 6 shows representative examples of the experimental and predicted progress curves for oxidation of the three selected compounds at different initial substrate and enzyme concentrations. Very good agreement is seen between the predicted and experimental data under all reaction conditions. Equation 1 does not take into account enzyme deactivation, and therefore predicted data after 20 h reaction time over predicted the experimental values for substrate concentrations higher than 100 mM in the case of all three compounds (data not shown).

3.4. Implications for bioconversion process design

Considering the kinetic parameter values in Table 4, the k_{cat} of compound **14** was 4 and 25 times higher than compounds **13**

and **7** respectively, but the Michaelis–Menten constant K_{amine} was 15 and 10 times higher respectively, which drastically affected the catalytic effectiveness of compound **14**. In terms of inhibition, the amine substrate was found to be the most inhibitory compound, greatly affecting compound **7** with an inhibition constant of 0.8 mM, while the $K_{i,amine}$ for compounds **13** and **14** were 4 and 6 times greater (less inhibitory) respectively. In this case substrate fed-batch operating would be recommended for compound **7** when attempting to achieve high space-time yields at larger scales.

Imine product inhibition was also found to be present, but to a much lower degree than for the substrates, with inhibition constants, $K_{i,imine}$, 1–2 orders of magnitude higher than the corresponding substrate inhibition constants (Table 4). For all the selected substrates, the oxygen inhibition constant, K_{i,O_2}, was found to be between 60 and 90 mM, which is 2 orders of magnitude above the aqueous O_2 saturation level indicating that oxygen inhibition was negligible under the reaction conditions examined. The kinetic models predict that increasing the dissolved oxygen
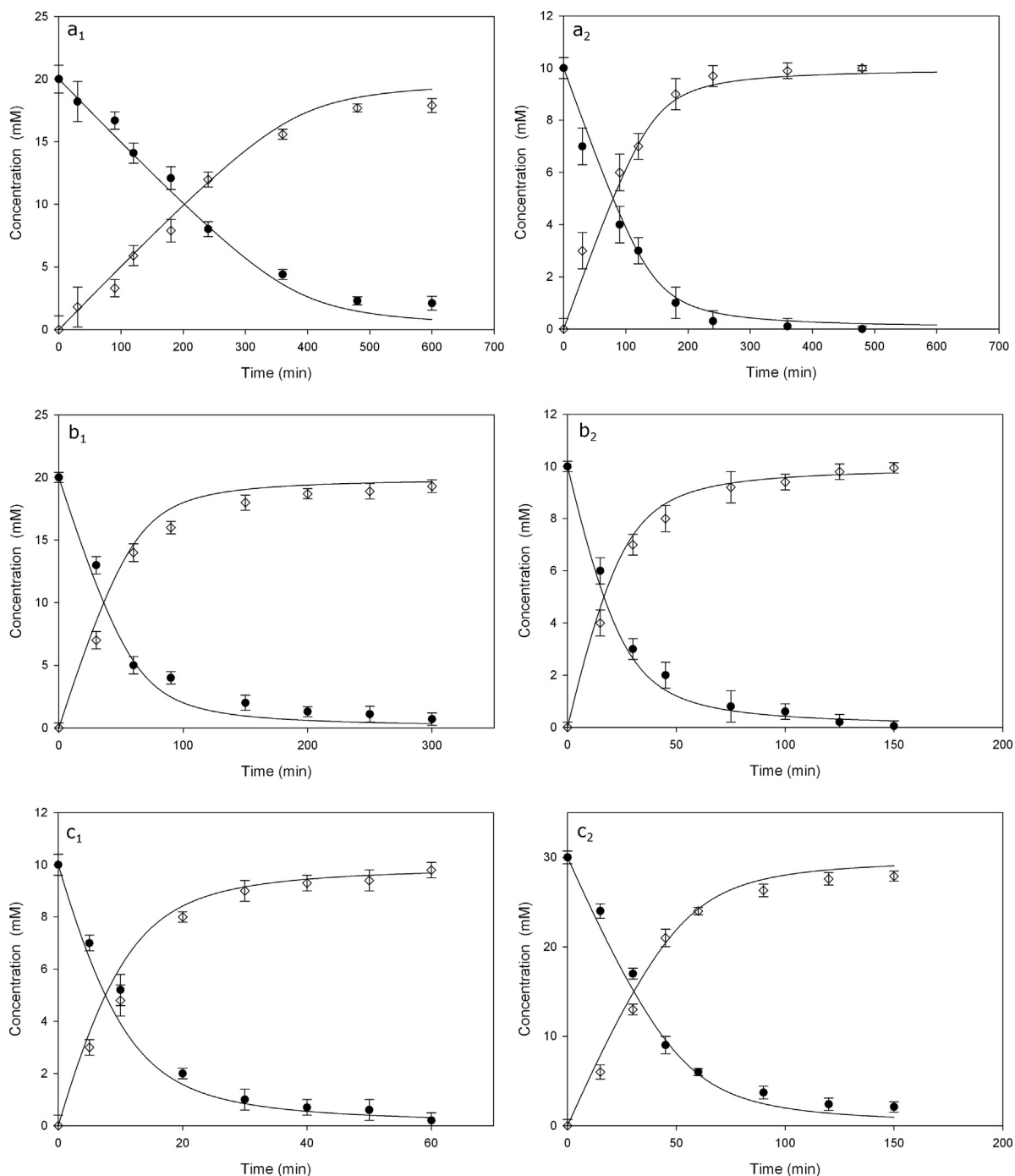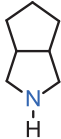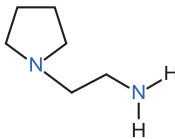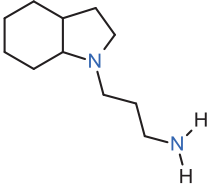

Fig. 6. Comparison of experimental and modelled bioconversion kinetics for the whole cell MAO-N-D5 mediated oxidation as a function of substrate and enzyme concentration showing amine (●) depletion and imine (◇) production: (a_1) 20 mM compound **7**, 66 units of MAO-N-D5, (a_2) 10 mM compound **7**, 49 units of MAO-N-D5, (b_1) 20 mM compound **13**, 6.5 units of MAO-N-D5, (b_2) 10 mM compound **13**, 3.3 units of MAO-N-D5, (c_1) 10 mM compound **14**, 6.5 units of MAO-N-D5, (c_2) 30 mM compound **14**, 3.3 units of MAO-N-D5. Experiments performed using the high throughput techniques described in Materials and Methods at 37 °C and pH 7.8 in 1 M phosphate buffer. Solid lines fitted based on Eq. (1) using the final kinetic parameters in Table 4. Error bars represent one standard deviation about the mean (n = 3).

Table 4
Final values of the apparent kinetic parameters determined for the selected substrates. **7**: 3-azabicyclo[3,3,0]octane, **13**: 1-(2 amino ethyl) pyrrolidine, **14**: 3-(2,3-dihydro-1H-indol-1-yl)propan-1-amine.

Substrate number	7	13	14
Chemical structure			
Rate constant: k_{cat} (mM h^{-1} units^{-1})	0.22	1.5	5.5
Amine Michaelis constant: K_{amine} (mM)	6.4	4.2	63.2
O$_2$ Michaelis constant: K_{O_2} (mM)	1.2	0.9	0.7
Amine inhibition constant: $K_{i,amine}$ (mM)	0.8	3.5	5.1
O$_2$ inhibition constant: K_{i,O_2} (mM)	57.1	72.6	89.5
Imine inhibition constant: $K_{i,imine}$ (mM)	54.5	170.0	300.3

concentration up to a saturation level of 1.25 mM would represent an approximately 4–5 fold reduction in the time required to reach full conversion. Hence it would be recommended to either sparge the bioreactor with pure oxygen, or an air-oxygen mixture (for non-flammable substrates), or to pressurize the vessel in order to achieve enzyme saturation with O$_2$ and maximize the reaction rate. This predicted effect due to increased oxygen levels has been previously observed using MAO-N-D5 with primary amine substrates [17].

Compared to kinetic constants reported in the literature for MAO-N-D5, the values of the Michaelis constant, K_{amine}, of compounds **7** and **13** are of the same order of magnitude as ones reported previously for other secondary amines, while that for compound **14** is one order of magnitude higher [24]. Compared to other constants found in the literature for primary amines using the wild type MAO-N-D5, the K_{amine} values for compounds **7** and **13** are at least 1 order of magnitude higher and 2 orders of magnitude higher than for compound **14** [17]. This could be explained because secondary amines are not natural substrates for the MAO-N-D5, and even with 4 mutations towards improved secondary amines activity [25], further improvement is needed achieve the Michaelis–Menten values and rate constants of MAO-N-D5 variants with primary amines.

Extensive studies can be found in the literature to identify inhibitors of MAO-A and MAO-B due to their importance for the treatment of depression, Parkinson's disease and several other disorders [36]. The identified inhibitors have also been found to severely inhibit MAO-N-D5, such as β-carboline derivatives and 1-methyl-4-phenylpyridinium where inhibition constants values ranged from 3 to 200 μM [17], which is closer to the value of $K_{i,amine}$ determined in this work for compound **7** (790 μM), while the inhibition constants for compounds **13** and **14** were one order of magnitude higher (Table 4).

Overall, the insights gained from the kinetic model generation suggest that amine substrate inhibition is a critical factor when considering MAO-N-D5 catalyzed bioconversions, which was in agreement with previous works focused on the MAO-N mediated oxidation of compound (**7**) [23] and of bicyclic amines [37]. Dissolved substrate concentrations above 100 mM severely affect the bioconversion rate and yield. At larger scale fed-batch operation and/or use of reactors in series will be necessary to make the conversions economically viable. The high throughput experimental methods and kinetic models described here are thus important tools to identify bottlenecks early and guide the selection of reaction engineering or biocatalyst engineering strategies to enhance overall productivity.

4. Conclusions

The MAO-N-D5 variant (Ile246Met/Asn336Ser/Met348Lys/Thr384Asn) studied here enabled the selective oxidation of secondary amines in 8 and 9 carbon rings, as well as primary ethyl and propyl amines attached to secondary amines of indolines and pyrrolidines. Those last two types of compounds were of special interest, due to the formation of new heterocyclic rings when oxidized by MAO-N-D5.

Our previously established high throughput microwell experimental platform and hybrid kinetic modelling methodologies enabled the rapid generation of full kinetic models for three MAO-N-D5 substrates based on the ping–pong bi–bi mechanism. The kinetic models for each amine substrate showed excellent agreement with experimentally determined progress curves over a range of operating conditions. The models indicated amine inhibition to be the main factor limiting reactor productivity, suggesting the need for fed-batch operation and enhanced dissolved oxygen concentrations in order to achieve the highest possible space-time yields.

References

[1] T. Narancic, R. Davis, J.N.K.E.O. Connor, Biotechnology (2015), Early published online.
[2] J.-M. Choi, S.-S. Han, H.-S. Kim, Biotechnol. Adv. (2015), Early published online.
[3] M.T. Reetz, J. Am. Chem. Soc. 135 (2013) 12480.
[4] A. Cázares, J.L. Galman, L.G. Crago, M.E.B. Smith, J. Strafford, L. Ríos-Solís, G.J. Lye, P.A. Dalby, H.C. Hailes, Org. Biomol. Chem. 8 (2010) 1301.
[5] N.J. Turner, A. Wells, ChemCatChem 6 (2014) 900.
[6] G. Sin, J.M. Woodley, K.V. Gernaey, Biotechnol. Progr. 25 (2009) 1529.
[7] M. Stitt, Y. Gibon, Trends Plant Sci. 19 (2014) 256.
[8] B. Chen, F. Baganz, J. Woodley, Chem. Eng. Sci. 62 (2007) 3178.
[9] B. Chen, M. Micheletti, F. Baganz, J. Woodley, G. Lye, Chem. Eng. Sci. 64 (2009) 403.
[10] L. Rios-Solis, N. Bayir, M. Halim, C. Du, J.M. Ward, F. Baganz, G.J. Lye, Biochem. Eng. J. 73 (2013) 38.
[11] M. Micheletti, G.J. Lye, Curr. Opin. Biotechnol. 17 (2006) 611.
[12] M. Halim, L. Rios-Solis, M. Micheletti, J.M. Ward, G.J. Lye, Bioprocess Biosyst. Eng. 37 (2014) 931.
[13] L. Rios-Solis, M. Halim, A. Cázares, P. Morris, J.M. Ward, H.C. Hailes, P.A. Dalby, F. Baganz, G.J. Lye, Biocatal. Biotransform. (2011).
[14] C.J. Du, L. Rios-Solis, J.M. Ward, P.A. Dalby, G.J. Lye, Biocatal. Biotransform. 32 (2014) 302.
[15] R.S. Islam, D. Tisi, M.S. Levy, G.J. Lye, Biotechnol. Bioeng. 99 (2008) 1128.

[16] L. Rios-Solis, P. Morris, C. Grant, A.O.O. Odeleye, H.C. Hailes, J.M. Ward, P.A. Dalby, F. Baganz, G.J. Dalby, Chem. Eng. Sci. 122 (2015) 360.
[17] S.O. Sablin, V. Yankovskaya, S. Bernard, C.N. Cronin, T.P. Singer, Eur. J. Biochem. 253 (1998) 270.
[18] K.E. Atkin, R. Reiss, N.J. Turner, A.M. Brzozowski, G. Grogan, Acta, Sect. Crystallogr, F. Struct, Biol. Cryst. Commun. 64 (2008) 182.
[19] R. Carr, M. Alexeeva, A. Enright, T.S.C. Eve, M.J. Dawson, N.J. Turner, Angew. Chem. Int. Ed. Engl. 42 (2003) 4807.
[20] K.E. Atkin, R. Reiss, V. Koehler, K.R. Bailey, S. Hart, J.P. Turkenburg, N.J. Turner, A.M. Brzozowski, G. Grogan, J. Mol. Biol. 384 (2008) 1218.
[21] C.J. Dunsmore, R. Carr, T. Fleming, N.J. Turner, J. Am. Chem. Soc. 128 (2006) 2224.
[22] P. Zajkoska, M. Rosenberg, R. Heath, K.J. Malone, R. Stloukal, N.J. Turner, M. Rebroš, Appl. Microbiol. Biotechnol. (2014).
[23] H. Ramesh, J.M. Woodley, J. Mol. Catal. B: Enzym. 106 (2014) 124.
[24] R. Carr, M. Alexeeva, M.J. Dawson, V. Gotor-Fernández, C.E. Humphrey, N.J. Turner, ChemBioChem 6 (2005) 637.
[25] V. Köhler, K.R. Bailey, A. Znabet, J. Raftery, M. Helliwell, N.J. Turner, Angew. Chem. Int. Ed. Engl. 49 (2010) 2182.
[26] J.Z. Baboo, J.L. Galman, G.J. Lye, J.M. Ward, H.C. Hailes, M. Micheletti, Biotechnol. Progr. 28 (2012) 392.
[27] M.M. Bradford, Anal. Biochem. 72 (1976) 248.
[28] B.H. Chen, E.G. Hibbert, P.A. Dalby, J.M. Woodley, AIChE J. 54 (2008) 2155.
[29] N.J. Turner, Chem. Rev. 111 (2011) 4073.
[30] J.W. Dubendorff, F.W. Studier, J. Mol. Biol. 219 (1991) 45.
[31] K.V. Gernaey, A.E. Lantz, P. Tufvesson, J.M. Woodley, G. Sin, Trends Biotechnol. 28 (2010) 346.
[32] O. Werbitzky, U. Daum, R. Bregy, US Patent US6476175 B2, 2002.
[33] Z. Wang, L. Li, US Patent US2014032229, 2014.
[34] S.D. Doig, S.C.R. Pickering, G.J. Lye, J.M. Woodley, Biotechnol. Bioeng. 80 (2002) 42.
[35] R.R. Deshpande, Y. Koch-Kirsch, R. Maas, G.T. John, C. Krause, E. Heinzle, ASSAY Drug. Dev. Technol. 3 (2005) 299.
[36] S.K. Al-Nuaimi, E.M. Mackenzie, G.B. Baker, Am. J. Ther. 19 (2012) 436.
[37] T. Li, J. Liang, A. Ambrogelly, T. Brennan, G. Gloor, G. Huisman, J. Lalonde, A. Lekhal, B. Mijts, S. Muley, L. Newman, M. Tobin, G. Wong, A. Zaks, X. Zhang, J. Am. Chem. Soc. 134 (2012) 6467.